



Article

Analysis of Visual and Vestibular Information on Motion Sickness in Flight Simulation

Ahmad Javaid ^{1,†}, Shahzad Rasool ^{1,†}  and Adnan Maqsood ^{2,*,†} 

¹ Immersive Technologies Lab, School of Interdisciplinary Engineering and Sciences, National University of Sciences and Technology, Islamabad 44000, Pakistan; iamajavaid@gmail.com (A.J.); shahzad.rasool@sines.nust.edu.pk (S.R.)

² Computational Aeronautics Lab, School of Interdisciplinary Engineering and Sciences, National University of Sciences and Technology, Islamabad 44000, Pakistan

* Correspondence: adnan@sines.nust.edu.pk

† These authors contributed equally to this work.

Abstract: Virtual reality (VR) is in its nascent technological advancement and market diffusion stages. Interestingly, the scientific exploration concerning the impact of non-isometric mapping disparities within visual–vestibular stimuli on motion sickness remains deficient. This investigation focuses on scrutinizing the visual–vestibular implications for motion sickness within the context of flight simulation. The developed motion platform, offering specific pitch and roll ranges of ± 16 and ± 17 degrees, respectively, was employed to induce varying ratios of simulated visual–vestibular cues. Involving a cohort of five participants, the study exposed them to two prevalent simulated mission profiles, subsequently assessing their motion sickness symptoms. Sixty responses were analyzed using the subjective assessment of the Simulator Sickness Questionnaire (SSQ). The findings reveal a reduction in cybersickness severity with congruent visual–vestibular stimuli in proportion to the variance observed among visual–vestibular coupling ratios. A comparative analysis of SSQ sub-categories demonstrates that disorientation holds the most significance in the hierarchy of motion sickness contributors, followed by oculomotor discomfort, with nausea manifesting as the least influential. This study can lead to situation awareness analysis by integrating VR-based flight-simulation setups in the formal training of pilots and UAV operators.

Keywords: virtual reality (VR); cybersickness; visual–vestibular cues; Simulator Sickness Questionnaire (SSQ)



Citation: Javaid, A.; Rasool, S.; Maqsood, A. Analysis of Visual and Vestibular Information on Motion Sickness in Flight Simulation.

Aerospace **2024**, *11*, 139. <https://doi.org/10.3390/aerospace11020139>

Academic Editor: Marco Sabatini

Received: 26 August 2023

Revised: 22 January 2024

Accepted: 26 January 2024

Published: 6 February 2024



Copyright: © 2024 by the authors. Licensee MDPI, Basel, Switzerland. This article is an open access article distributed under the terms and conditions of the Creative Commons Attribution (CC BY) license (<https://creativecommons.org/licenses/by/4.0/>).

1. Introduction

Virtual reality (VR) is an immersive technology for professional and entertainment flight-simulation setups. However, VR head-mounted displays (HMDs) have inherent drawbacks, such as virtual locomotion, creating a sense of motion without corresponding physical movement. This asynchronization between visual and physical input can potentially cause motion sickness [1]. For example, when the user is sitting or standing still in real life while the VR headset simulates the feeling of making sudden turns in a flight simulation, it can cause a disconnect between what the eyes are seeing and what the body is feeling. This results in feelings of nausea, dizziness, and discomfort [2]. To minimize the potential for motion sickness related to virtual locomotion and vection, VR headsets can be synchronized with motion platforms [3,4]. In this research, the mitigation of adverse effects of VR headsets is studied by augmenting a flight-simulation setup with a low-fidelity motion platform. Mapping visual cues over vestibular cues generates a more realistic and immersive user experience that mitigates the risk of motion sickness.

VR-based motion platforms support pilot–simulator interaction by duplicating the dynamic behavior of an aircraft under multiple missions, tactile scenarios, and flight parameters [5]. Multiple channels of information exchange between the operator and

the simulation engine make VR-based flight simulators immersive and interactive. The navigational haptic force feedback provided through a control stick generates visual and acoustic gain through the HMD, while the angular rotation of the motion platform generates vestibular output. After analyzing the feedback from the visual, vestibular, haptic, and acoustic systems, the pilot operates the flight simulator using the control stick, forming a closed-loop scenario, as shown in Figure 1. This sensory information enhances situational awareness and optimizes pilot control. In VR flight simulators, these cues depend on the aerodynamic load and force calculations from the game engine to the motion drive system. For a high-fidelity immersive flight simulator, the sensory simulations produced artificially through the game engine must be synchronized, replicating the real flight environment to mitigate VR sickness. This research uses a motion platform to analyze visual–vestibular effects on motion sickness in flight simulation.

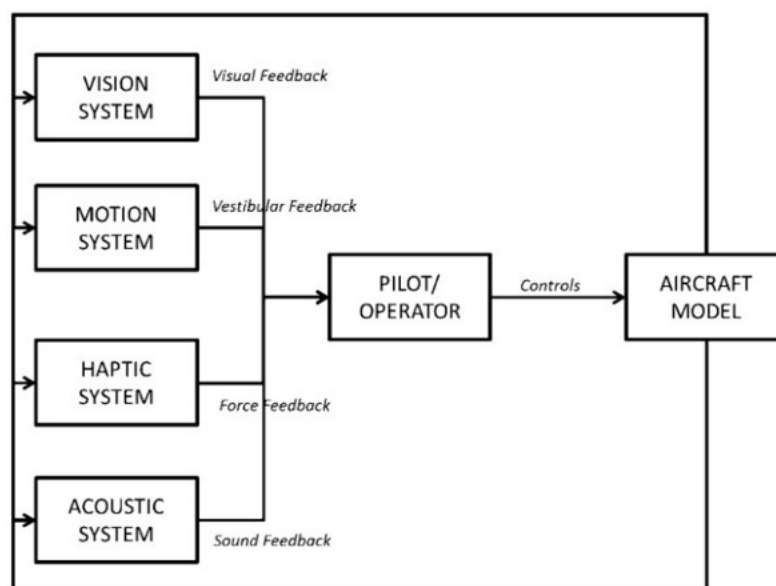


Figure 1. Closed-loop stimulus.

Effect of Sensory Interface on Motion Sickness

VR motion sickness, sometimes called cybersickness, occurs when a user experiences unpleasant sensations such as drowsiness, nausea, disorientation, and eye strain. This happens when the user is in an immersive VR environment where visually-induced illusory cues provide optical flow information without corresponding motion cues [6–8]. In VR simulators, patterns of specific objects such as roads, runways, buildings, clouds, and other external elements generatevection—a sensation of self-motion. These patterns provide visual cues about the user’s dynamic condition with a specific acceleration in a particular direction. However, since the user is stationary, the vestibular organs indicate the static condition of the user. The sensory conflict between optical-motion cues leads to cybersickness.

The degree of head movement constraints during VR exposure affects the severity of cybersickness. One way to reduce these constraints is by integrating positional trackers with a VR headset, which allows the user to physically move in the real world while exploring the virtual environment [9]. This provides vestibular information that matches the visual cues of the virtual environment and reduces the conflict between sensory modalities. Studies have compared cybersickness with various locomotion techniques. For example, Keshavarz et al. [7] found that cybersickness was significantly reduced when users navigated through physical movements compared to a static condition generated with a game controller. Lisa et al. [10] observed thatvection was more apparent when users did not interact with virtual stimuli in the real world. However, Golding [11] found no difference in the level of cybersickness between physical movements in the real world or joystick-

based movements that duplicated the visual cues of the VR environment. Nevertheless, better task performance was observed when users moved freely physically. The level of synchronization between active head movement and optical flow determines the severity of cybersickness, and it increases when the optical flow moves in the same direction as the physical movement [9].

Several researchers have studied the relationship between simulated motion cues and motion sickness. Some studies have found a positive correlation between the two [12], while others have found no correlation [13] or a negative correlation [14]. Dziuda et al. [15] explained that motion-simulated environments should closely resemble real-world movements to avoid inducing additional conflict and a negative correlation with motion sickness. Studies have shown that a 6-degree-of-freedom (DoF) visually synchronized motion platform induces less sickness than a static platform that only provides visual cues [16]. Adrian et al. [17] established a link between presence and cybersickness by simulating three visual-vestibular synchronization conditions and recording scores through the Simulator Sickness Questionnaire (SSQ), Misery Scale (MISC), and Joyfulness Scale (JOSC). They found that synchronized visual-vestibular motion induces less cybersickness than stationary conditions featuring only visual cues and antiphase virtual viewport motion to physical rotation. However, there could be carry-over effects such as habituation and sensitization. Some researchers have used a multi-screen visualization environment instead of a head-mounted display (HMD) to generate the visual-motion stimulus, covering the user's field of view. Hepers et al. [18] designed a test bed using immersion square technology to conduct a cognitive and workload analysis under physical and psychological stress factors. They used a prototype bike mounted on a Stewart platform and FIVIS simulation software (FIVISim) to simulate realistic tracks, turns, and external forces exerted on the bicycle on a 120° projection screen.

Some studies observed that implementing a motion platform and visual cues induced more discomfort and sickness in individuals than utilizing a static platform. Specifically, Dziuda et al. [15] noted that the physical-motion system heightened the experience of discomfort and oculomotor issues, which could persist for a significant duration of time. Additional research has shown that simulator sickness can be mitigated through situational awareness and acclimatization to specific environments [19]. For instance, Hodder and Howarth [20] discovered that daily exposure to a virtual simulator environment for ten days could reduce VR and motion sickness. Additionally, several factors, such as high frame rate rendering, synchronization of sensory cues, short-persistence visual displays, and consistency between physical motion and optical flow, have been reported to significantly minimize or even eliminate VR sickness [21–24].

Tal et al. [25] conducted a study to mitigate sea sickness in a boat simulator by introducing an earth-referenced visual horizon. The results demonstrated that implementing an artificial, simplified visual horizon within a synchronized environment effectively reduced perceived motion sickness. This hypothesis was also supported by Bos et al. and Feenstra et al. in their respective studies [26,27]. Additionally, studies conducted in VR environments found that employing a self-referenced frame, limiting the field of view, and including a body part could alleviate symptoms of motion sickness [28–31].

2. Design of Motion Platform

A mechanical device's degrees of freedom (DoF) are related to its cost. Achieving a high DoF in flight simulators is increasingly expensive. Thus, to avoid a complex mechanical design and high price, the design of the flight simulator was restricted to only two degrees of freedom, i.e., roll and pitch motion. For visual and vestibular human-machine interaction, the motion system included a communication module, control software module, and control system module. The input devices, i.e., HOTAS joystick and throttle, were integrated with the simulator platform, and the game engine was installed on multi-core processors and GPUs. Steam was installed on high-performance workstations to run virtual

reality flight simulations on Oculus Rift S. The system's overall methodology is elucidated in Figure 2.

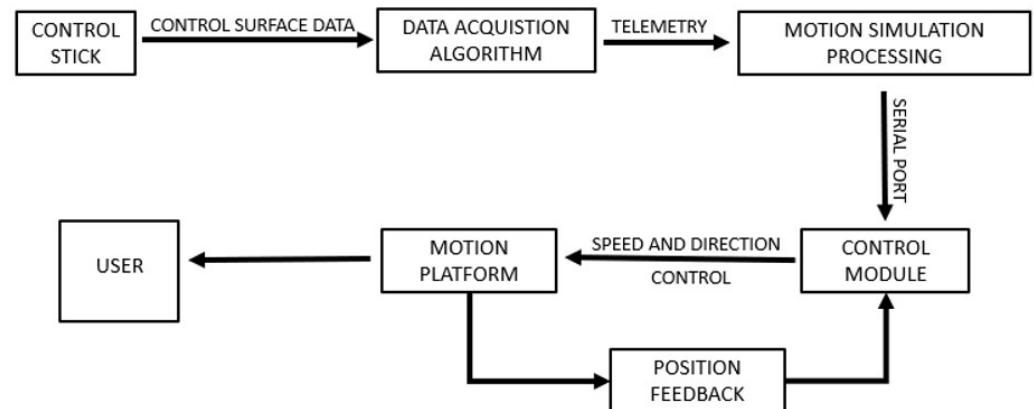


Figure 2. The architecture of the motion platform.

The user interacts with the flight simulator using a control stick, offering input commands. The simulation model subsequently processes these input commands. Within the motion-control framework, encompassing motion-control software and a communication module, data undergo translation through washout filters, referred to as the motion cues algorithm. These filters assimilate feedback from position encoders, converting motion-related information into electrical voltage signals. These signals regulate the roll and pitch motions of the motion platform, thereby producing vestibular cues discernible to pilots. The washout algorithm evaluates the analog signal, facilitating the generation of pertinent output motion commands for the controller.

2.1. Communication Module

X-plane establishes communication with an external interface, specifically, MATLAB, 2023b[®] Simulink, utilizing the UDP communication protocol. The transmitter module is responsible for conveying aircraft state details through data packets. Each data packet comprises four bytes and is organized into nine distinct categories. Therefore, a comprehensive assessment of the aircraft's navigation state necessitates the analysis of a cumulative 293-byte dataset. On the receiver side of the communication system, an Arduino[®] UNO device (BCMI, Strambino, Italy) decodes the incoming high-speed data stream, extracting telemetry information and aircraft control surface parameters. The received datasets are deconstructed into discernible control variables. This decoding function then converts the data matrix of packets into a singular floating-point value. Subsequently, these floating-point numbers are further transformed into double-precision values, which govern the motion the flight simulator's synchronized roll and pitch attributes.

2.2. Mechanical Design

For a 2-degree-of-freedom (2 DoF) configuration, a pair of actuators is aligned along the y-axis. These actuators move correspondingly and inversely to produce pitch and roll motions. The arrangement involves the integration of a stationary lower base and an upper movable frame in a cascaded fashion. A universal joint is coupled with a lower floor and upper edge. The location of the universal joint depends on the user's center of gravity. Two connecting rods connected to the motor lever at 90° hold the upper frame parallel to the lower base. Swivel joints are connected at both ends of the rods. They remove unnecessary and unwanted strain when the motion platform rotates in the roll and pitch directions. The maximum angular workspace in the roll and pitch directions was found to be ±16° and ±17°, respectively.

It is preliminary to determine the center of gravity (CG) concerning the user’s sitting posture, as mentioned in Figure 3a, before connecting the lower base to the upper portion of the platform, ensuring motion around a fixed reference point. Thus, the vertical placement of the connecting rods was made close to the center of gravity. For offset compensation of the center of gravity, the seat was placed a few inches back from the center of connecting rods.

Another significant parameter in the motion platform’s design involved assessing the force exerted by the motors on the platform and the resultant torque generated. This analysis was crucial to ensure the platform could physically accommodate a load capacity of 120 kg, encompassing both the user and the motion platform.

The other two forces acting on the motors were radial and axial. The radial force was in line with the lever of the motor, whereas the axial force was parallel to the motor’s shaft. These forces were dependent upon the mounting geometry of the actuators. Through static force analysis, $\rightarrow F_{rad}$ and $\rightarrow F_{ax}$ were calculated. All the calculations were performed under two assumptions: (1) the universal joint remains static and (2) the material design is rigid.

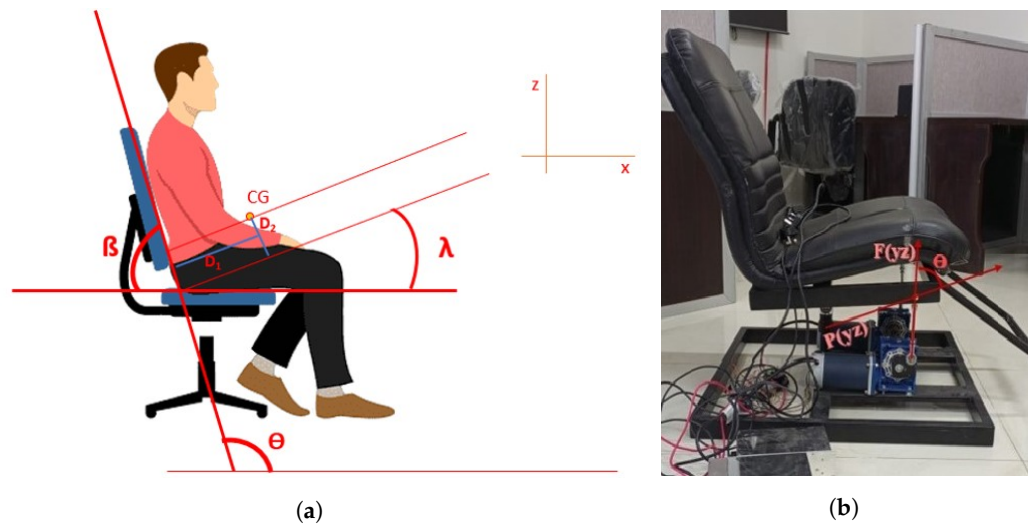


Figure 3. (a) Reference user sitting posture for the center-of-gravity calculation. (b) Equivalent forces acting on the motion platform.

The equivalent pitch force and torque were calculated using Equation (1) and Equation (2), respectively.

$$\rightarrow F_{pitch} = \rightarrow F \sin(\theta_{yz}) \tag{1}$$

$$\tau_{pitch} = \left| \rightarrow F_{pitch} \right| \rightarrow P_{yz} \tag{2}$$

Similarly, the roll torque and force can be calculated using Equation (3) and Equation (4), respectively, as illustrated in Figure 3b.

$$\rightarrow F_{roll} = \rightarrow F \sin(\theta_{xz}) \tag{3}$$

$$\tau_{roll} = \left| \rightarrow F_{roll} \right| \rightarrow P_{xz} \tag{4}$$

2.3. Electrical Design and Mathematical Modeling

The electrical system design was sequenced after the flight simulator’s structural assessment and load analysis. This design encompasses a unified module functioning as the central control hub for the flight simulator. This module comprises an Arduino unit, two 30A IBT2 motor control drivers (iHaospace, China), two 24V 21A power supplies denoted S-500-24 (Wenzhou, China), and two Hall-effect potentiometer angle encoders (Digikay, Birmingham, England). These encoders provide positional feedback for motor operation.

At the rear end of the motion platform were two 24 V DC worm gear motors strategically engaged in enhancing torque generation for roll and pitch rotations and maintaining the flight simulator in a stable orientation.

The transfer function of the motion platform is obtained through the ratio of output speed and input voltage under the assumption that the torque load is constant:

$$\frac{\omega_m(s)}{V_a(s)} = \frac{K_m}{(R_a + sL_a)(Js + B + T_L) + K_mK_b} \quad (5)$$

where $\omega_m(s)$ is the angular speed of the motion platform, $V_a(s)$ is the input voltage to the system, K_m is the motor constant, R_a is the armature resistance, L_a is the armature inductance, B is the damping coefficient, T_L is the torque load of the motor, J is the equivalent inertial load, and K_b is the back EMF constant of the motor.

The state-space representation of the motion platform can thus be represented as

$$\begin{pmatrix} \dot{i}_S(t) \\ \dot{\alpha}(t) \\ \dot{\omega}(t) \end{pmatrix} = \begin{pmatrix} -\frac{R_a}{L_a} & 0 & -\frac{k_g}{L_a} \\ 0 & 0 & 1 \\ \frac{k_g}{J_{eq}} & 0 & -\frac{B}{J_{eq}} \end{pmatrix} \cdot \begin{pmatrix} i_S(t) \\ \alpha(t) \\ \omega(t) \end{pmatrix} + \begin{pmatrix} \frac{1}{L_a} & 0 \\ 0 & 0 \\ 0 & -\frac{1}{J_{eq}} \end{pmatrix} \cdot \begin{pmatrix} E_a(t) \\ T_L(t) \end{pmatrix} \quad (6)$$

where K_g is the internal gear reduction and J_{eq} is the equivalent inertia of the motion platform.

We consider the system's closed-loop response, where the angular displacement of the motor is dependent on the analog value of the position encoder. It was necessary to design a controller that tracks the position encoder's real-time response concerning the aircraft's aerodynamic characteristic, depicted through the angular motion of the actuator. The mathematical model of the motion platform was simulated through MATLAB Simulink, and a closed-loop response was observed, represented by thinner lines in Figure 4. The closed-loop system generates a damping response with an 86.9% overshoot from the steady-state value with a maximum angular rotation of 40 rpm and a transient response of about 3.24 s. The damped response of the system was optimized using a PID controller. The output of a PID controller is calculated based on feedback error in the time domain as

$$u(t) = K_p e(t) + K_i \int e(t) dt + K_d \frac{de}{dt} \quad (7)$$

where K_p , K_i , and K_d are the gain parameters of the PID-based washout algorithm. The washout algorithm was applied in certain conditions where the simulator reached its maximum motion limits. In Condition C2, the simulator's physical rolling and pitching motion did not reach its maximum limits, so the washout algorithm was not applied. The washout algorithm was applied repeatedly in a fraction of a second in the physical rolling and pitching motion. Therefore, specifying certain instances in which the washout algorithm was applied is challenging.

The thicker line in Figure 4 represents the PID-tuned response of the system. It is explicit that the PID controller has refined the system's transient response and improved the steady-state error by reducing the damping oscillations in the system. The tuned values of the PID controller were imported into the motion-control software, i.e., Simtools. Simtools and the microcontroller link the communication module with the motion platform. As the motion-control software extracts real-time parameters from the X-plane, such as force, speed, telemetry, and shifting gear, all these parameters are integrated into a standardized data packet and exported to the microcontroller through a communication module to control the pitch and roll attributes of the flight simulator. The software's primary data output was tracking the actuators' position demand through the Hall-effect position encoder potentiometer to simulate real-time flight in the pitch and roll directions.

To replicate a realistic human sensory experience, the motion-control algorithm was enhanced with a series of motion filters, followed by meticulous tuning within the constraints of the flight simulator's physical capabilities. Introducing a hysteresis loop addressed

the gradual transitions in inertial cues, specifically, pitch and roll motion. A recurring issue observed was the simulator becoming wedged at its extremities, failing to reestablish its initial reference position. To counter this, implementing a traction-loss mechanism facilitated the smooth repositioning of the simulator from its maximum or minimum range of motion back to its reference point.

The PID-based washout algorithm, incorporating parameters like filtering and saturation limits, was employed to surpass the inherent physical constraints of the motion platform. When the simulator approaches its operational limits dictated by game inputs, the motion platform effectively reverts to its initial stabilized configuration without necessitating modifications to the game parameters. This iterative process, enhanced by filtering, contributes to the simulator's overall physical threshold and authenticity. Realignment towards the reference position is executed with minimal velocities, approximately 0.04 m/s, thereby mitigating the incongruence between visual and vestibular cues and minimizing discrepancies in human sensory perception. The saturation limits act as a safeguard, preventing excessive output values that the motion platform may not be able to achieve, ensuring user comfort and safety.

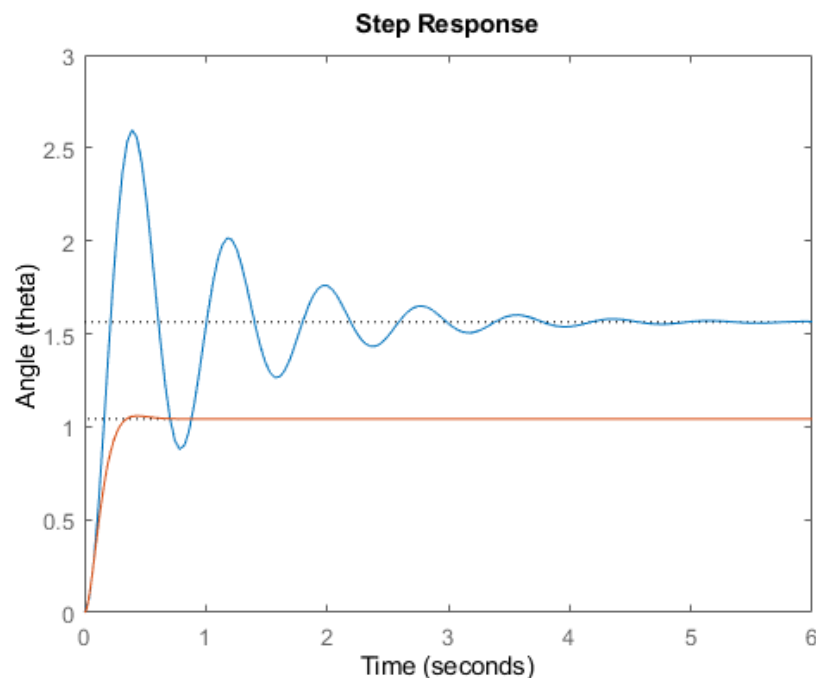


Figure 4. PID tuned response.

3. Motion Sickness in Virtual Flight Simulation

According to sensory conflict theory, motion sickness arises due to asynchronization between visual and vestibular cues. A discrepancy in these cues within the internal stimulus of the central nervous system (CNS) can lead to nausea, headache, dizziness, vertigo, and other symptoms [32]. Several studies have defined the relationship between simulated motion cues and motion sickness. Some studies have reported a positive correlation, while other studies have no correlation [13] or a negative correlation [14] explicitly. Fewer computational algorithms and motor and vehicle kinematics limitations induce additional conflict and derive a negative correlation between motion sickness and the motion platform [33]. The quantitative score of correlation is recorded through the Simulator Sickness Questionnaire (SSQ), Misery Scale (MISC), and Joyfulness Scale (JOSC). Studies have reported that synchronized visual–vestibular motion induces less cybersickness compared to stationary conditions featuring only visual cues and the anti-phase virtual viewport motion to the physical rotation. Carry-over effects such as habituation and sensitization could be a drawback. This study was conducted continuously over a short duration due to minimal break

time between two simulated conditions. Besides HMD, a visual-motion stimulus can be generated using a multi-screen visualization environment covering the user's field of view.

Several investigations have noted that introducing a motion platform and visual cues can lead to more discomfort than static scenarios. Dziuda et al. [15] discerned that the presence of physical motion systems contributed to heightened discomfort and oculomotor challenges, with users experiencing lingering after-effects. Strategies such as rendering at high frame rates, aligning sensory cues, employing short-persistence visual displays, and ensuring linear congruence between physical motion and optical flow have been proposed to significantly alleviate or even eliminate VR sickness.

The present study adopts a distinctive approach by designing a 2-degree-of-freedom (2DoF) flight simulator. The focus is investigating strategies and their alignment in ameliorating VR sickness, which arises from the asynchronization between visual and vestibular cues. This study seeks to contribute to understanding effective methods to counteract VR sickness induced by motion and vestibular cue coupling.

3.1. Simulator Sickness Questionnaire

Generally, the amount of cybersickness can be determined through subjective assessments and questionnaires. The Simulator Sickness Questionnaire is the most frequently used among all studies [34]. It divides motion sickness symptoms into three categories: disorientation (D), oculomotor (O), and nausea (N). Disorientation includes symptoms such as vertigo, dizziness, and difficulty focusing. Oculomotor symptoms include headaches, blurred vision, and eyestrain. Nausea has increased salivation, stomach awareness, and blurred vision. The profile of cybersickness is characterized based on the severity and frequency of these symptoms, with disorientation at the top, followed by nausea and oculomotor last, often called a D>N>O profile [35]. There is a difference between the profile of cybersickness and traditional motion sickness. Sea sickness has an N>O>D profile, simulator sickness has an O>N>D profile, and space sickness has an N>D>O profile. Moreover, cybersickness symptoms are reportedly much more severe than traditionally perceived motion sickness symptoms.

Beyond the cybersickness manifestations outlined within the Simulator Sickness Questionnaire, additional physiological symptoms emerge, including heightened heart rate, altered eyeblink frequency, fluctuations in EEG readings and temperature, escalated tachygastric power, decreased bradygastric power, pulse amplitude variations, and alterations in breathing rate [9,36]. The subjective evaluation of these physiological indicators verifies the extent of cybersickness and reflects the level of fidelity achieved by the motion simulator. The primary objective of this study is to assess motion sickness through the Simulator Sickness Questionnaire, thereby contributing to a comprehensive understanding of the phenomenon.

3.2. Apparatus

The experimental setup used in this study consisted of the 2DoF flight simulator, an HMD system (Oculus Rift S), and a HOTAS controller. The flight simulator generated roll and pitch motion at an angle of $\pm 16^\circ$ and $\pm 17^\circ$, respectively. The HMD system is an integrated stereoscopic head display package with onboard position-tracking sensors and hand controllers. The features of the HMD system are presented in Table 1. The response of the 2DoF flight simulator was controlled through the HOTAS controller. Users experienced vestibular cues from the motion platform and visual cues from the Oculus Rift S. The participants were seated on the chair at the center of rotation of the flight simulator. The back of the chair was used to constrain the user's physical head orientation and rotation. The offset rotation of the flight simulator was set to zero to perceive actual inertial cues corresponding to the visual sensory output. The software Xplane 11 was used for the visual sensory interface. Visual information of flight plans over buildings in Chicago while sitting in the cockpit of a Boeing 777 was simulated.

Table 1. Features of Oculus Rift S.

Type	Standalone
Resolution	1832 × 1920 (per eye)
Refresh Rate	90 Hz
Motion Detection	6 DoF
Controls	Oculus Touch

3.3. Participants

The case study recruited 5 participants (three female and two male) aged between 22 and 27 (mean = 24, SD = 1.22). All users were students enrolled in the Systems Engineering program. All participants were healthy and had no prior illness. To analyze motion sickness, overall, 60 experiments were conducted with a sufficient number of participants [37]. As fatigue induces early symptoms of vection and motion sickness, an experiment was conducted in the 2nd quartile of the day [38]. Overall, 40% of the participants skipped breakfast but consumed surplus calories during the last meal [39], as continuous prolonged VR exposure results in motion sickness. To mitigate the influence of motion sickness from the prior treatment condition on the subsequent one, a 30 min break was observed by each participant after every experiment [40].

3.4. Experimental Conditions

The experiment was designed to subjectively assess motion sickness across varying degrees of physical motion. Participants were positioned within the 2-degree-of-freedom (2DoF) flight simulator setup, where they were exposed to sensory stimuli simulating flight scenarios. Each participant engaged with two mission profiles, each limited to a distinct axis of rotation (pitch or roll). Comprehensive mission profile specifications can be found in Figures 5 and 6. Before the flight, subjects were instructed to adjust their field of sight to align parallel to the horizon, effectively minimizing additional discrepancies in visual feedback. Acknowledging that subjective pilot handling qualities influence mission profiles and subsequent motion sickness experiences is essential. To counterbalance this impact, participants were intentionally not given manual flight control. A passive control environment was observed with an expert performing the designated mission profile and a participant experiencing flight simulation through a VR headset, as illustrated in Figure 7. Although a dedicated viewpoint allowed the flyer to monitor the turn angle and flight attitude, the potential for human error persisted. To address this, a considerable number of user reviews were systematically documented. As the aircraft navigated through each mission profile, as illustrated in Figures 5 and 6, participants perceived visual cues through stereoscopic displays in the VR headset and vestibular information through the motion simulator. This multi-sensory information was experienced across six diverse ratios, with one being a synchronous condition and the remaining five asynchronous conditions, as depicted in Figure 8. The details of the asynchronous conditions are explained in C1 to C5. These six ratios were individually simulated across two mission profiles—roll and pitch mission profiles—resulting in 12 motion profiles, as outlined in Table 2. The specific breakdown of the six ratios of inertial and visual cues is as follows:

- C1 (No Motion): No-motion condition; only visual cues are simulated with no reference motion signals.
- C2 (Log): Logarithmic condition, in which a tenfold increase in physical motion is observed against visual input.
- C3 (Exp): Exponential condition; an exponential increase in physical motion against visual input is observed.
- C4 (Gain ×0.5): Scaled-down condition, in which visual inputs are rendered to the motion simulator with a gain of 0.5.

- C5 (Gain $\times 2$): Scaled-up condition, in which visual inputs are rendered to the motion simulator with a gain of 2.
- C6 (Synchronous): Synchronous condition; motion cues are perfectly synchronized with visual cues.

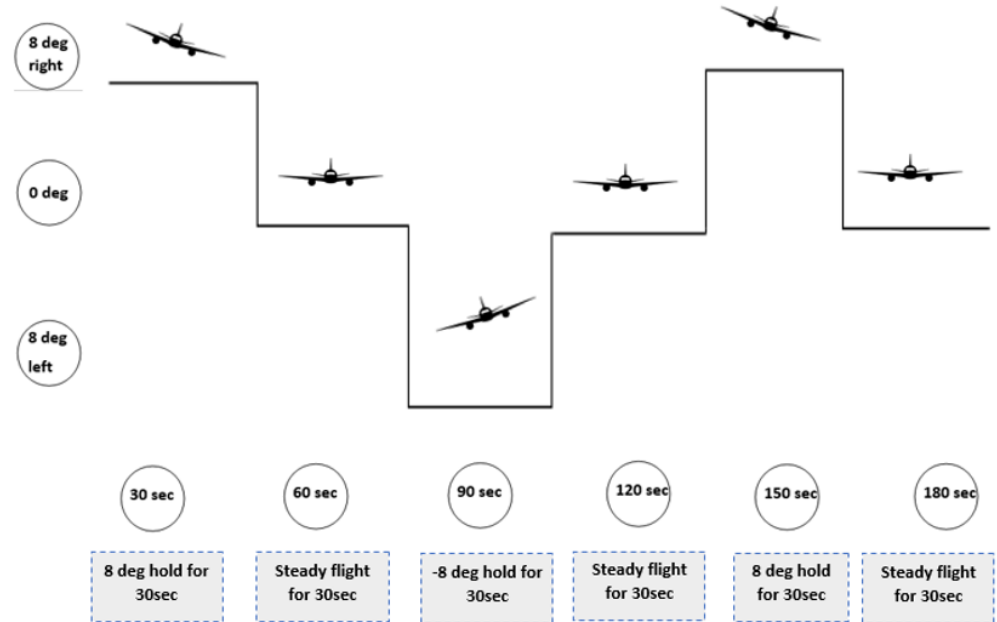


Figure 5. Simulated-mission profile for roll motion.

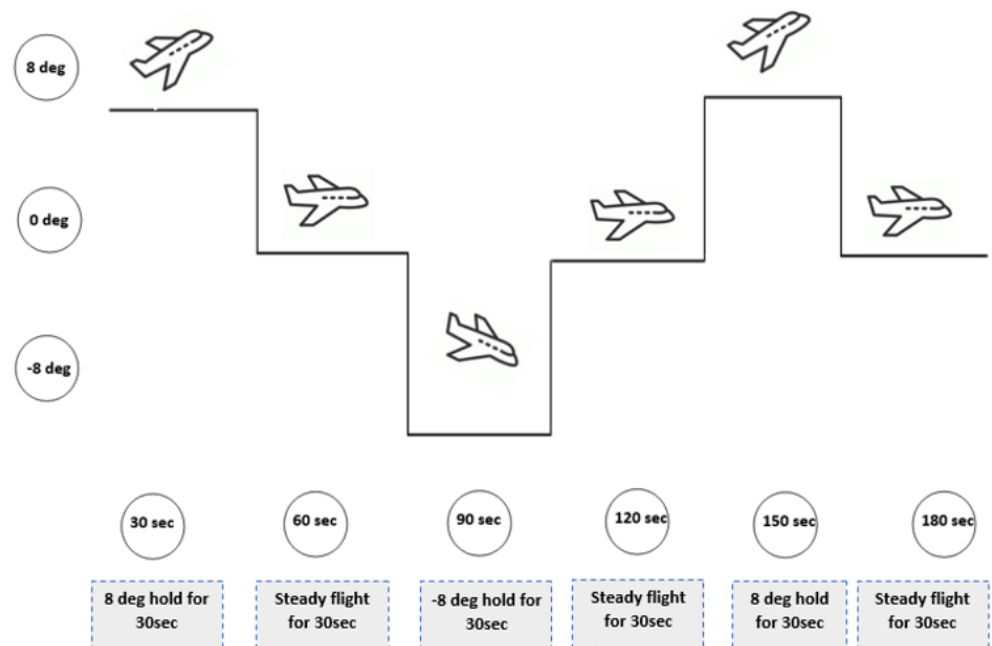


Figure 6. Simulated-mission profile for pitch motion.



Figure 7. A user (left) experiencing mission profile with a pilot (right) in command of flight controls.

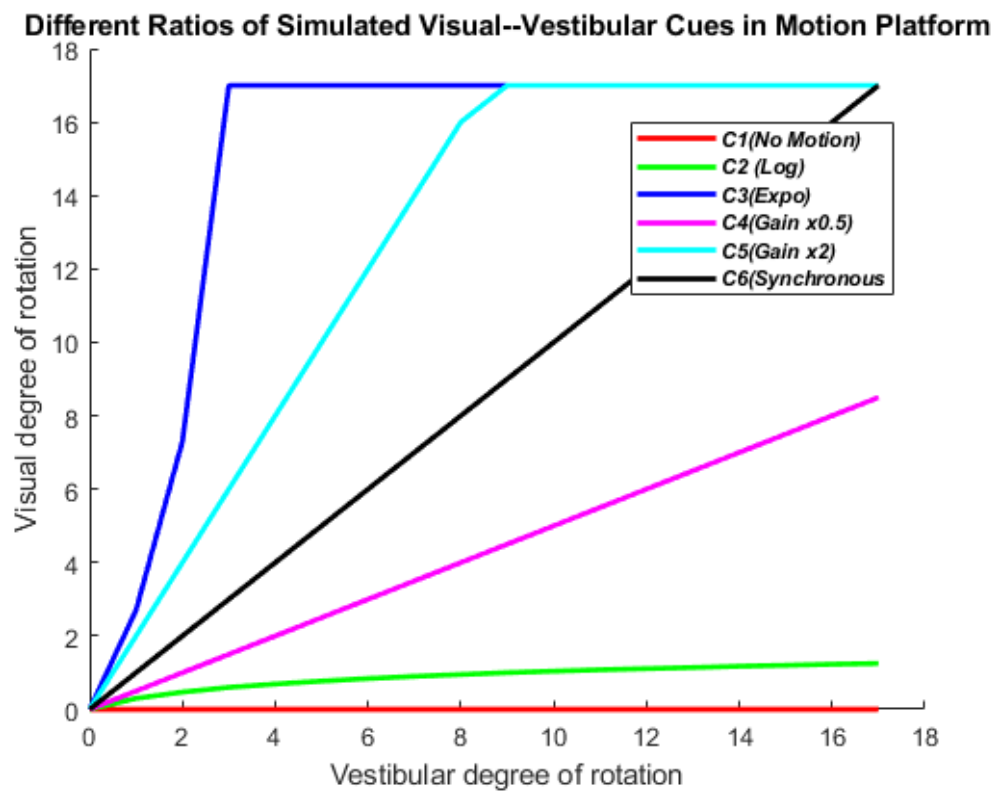


Figure 8. Variable ratios of visual-vestibular conditions.

All six conditions of visual–vestibular cues were replicated separately for both mission profiles, yielding 12 distinct motion profiles, as outlined in Table 2. Following each mission profile, all five participants evaluated their perceived motion sickness severity using a motion sickness questionnaire. Thus, a large data group was analyzed against the hypothesis (5 participants \times 12 mission profiles). These collected responses were subjected to rigorous statistical analysis to ascertain the peak instances of motion sickness experienced across the various simulated conditions.

Table 2. A total of 12 motion profiles across two mission profiles.

S. No	Motion Profiles
1	C1 (No Motion)/Pitch mission profile
2	C2 (Log)/Pitch mission profile
3	C3 (Exp)/Pitch mission profile
4	C4 (Gain \times 0.5)/Pitch mission profile
5	C5 (Gain \times 2)/Pitch mission profile
6	C6 (Synchronous)/Pitch mission profile
7	C1 (No Motion)/Roll mission profile
8	C2 (Log)/Roll mission profile
9	C3 (Exp)/Roll mission profile
10	C4 (Gain \times 0.5)/Roll mission profile
11	C5 (Gain \times 2)/Roll mission profile
12	C6 (Synchronous)/Roll mission profile

It is postulated that the incorporation of motion cues alongside visual information should lead to a reduction in the severity of motion sickness. No predetermined hypothesis exists concerning the level of motion sickness severity about various ratios of visual–vestibular conditions. However, it is conjectured that a synchronized visual–vestibular state may result in decreased motion sickness. Two distinct hypotheses were formulated in conjunction with the experimental setup and the diverse modes of visual–vestibular conditions:

First Hypothesis: Introduction of motion cues alongside visual cues will reduce motion sickness. Second Hypothesis: Motion sickness will depend on the correspondence of visual and motion cues.

To facilitate the case study, two questionnaires were devised—the pre-VR questionnaire comprised closed-type queries aimed at gathering general user information. Since factors like fatigue levels, energy expenditure, and sleep patterns can influence motion sickness, user responses were recorded for each parameter. The post-VR experience questionnaire was designed to gauge motion sickness severity through the motion sickness questionnaire. After each experiment, the users were asked to answer the motion sickness questionnaire [41]. As the study encompassed 12 motion profiles (6 conditions for each mission profile), an independent questionnaire was developed for each motion profile, summing to 12 questionnaires for each participant. The roll mission profile simulation organized responses into six columns, each representing the response generated against the individual ratio of visual–vestibular cues. The user feedback generated during the roll mission profile was subjected to statistical analysis using one-Way ANOVA. Similarly, feedback from the pitch mission profile simulation yielded six population columns that were analyzed. Consequently, 60 responses were captured and analyzed across five participants.

3.5. Analysis Tools

The subjective evaluations conducted by each participant across the 12 distinct conditions were examined to derive insights into the relationship between motion sickness

and visual–vestibular sensory input. The analysis of variance (ANOVA) technique was employed on the Simulator Sickness Questionnaires (SSQ) to analyze the score of motion sickness across 12 motion profiles. Multiple independent models were also constructed using distinct variables, which encompassed the nausea (N) score, disorientation (D) score, oculomotor (O) score, and cumulative SSQ score. These separate models were developed to analyze the score of nausea (N), disorientation (D), and oculomotor (O) across 12 distinct conditions. All these scores were computed using standardized formulas. Table 3 succinctly presents the statistical outcomes of a score of motion sickness for each mission profile across the six conditions (C1, C2, C3, C4, C5, C6).

Table 3. Statistical outcome of a score of motion sickness in pitch and roll mission profile across all six conditions.

Motion: Visual	Pitch		Roll	
	Mean	S.D	Mean	S.D.
C1 (No Motion)	23	4	31	8
C2 (Log)	22	5	28	5
C3 (Expo)	16	4	18	3
C4 (Gain ×0.5)	17	5	20	4
C5 (Gain ×2)	19	3	24	4
C6 (Synchronous)	13	3	15	2

4. Results and Discussion

The sizeable variance within individual groups underscores the significant impact of altering the visual–vestibular cue ratio on the manifestation of motion sickness.

4.1. Main Effect of Motion Across Pitch and Roll Profiles

A statistical analysis was conducted to ascertain the motion sickness scores in response to visual stimulus exclusively and the concurrent amalgamation of visual–vestibular sensory stimulation for pitch and roll mission profiles. A one-way ANOVA was performed to determine whether the addition of motion cues to the user’s visual experience significantly affects the motion sickness score, revealing *p*-values of 0.029 and 0.009 for the roll and pitch mission profiles, respectively. The statistical analysis of these two separate models is summarized in Table 4. The range of effect sizes within parameters of small (=0.01), medium (=0.06), and large (>0.14) functions as a reference for interpreting the results.

Table 4. Statistical analysis of motion sickness scores for visual and visual–vestibular stimuli across roll and pitch mission profiles.

<i>p</i> -Value	Effect Size	F-Value
Roll Mission Profile		
0.029	0.34	7.00
Pitch Mission Profile		
0.009	0.31	11.76

The central tendency of a score of motion sickness experienced by the users with and without motion stimulus is depicted in Figure 9. The blue box plots show the score of motion sickness for the roll mission profile, whereas the red boxes represent the score of motion sickness for the pitch mission profile. The dispersion of the data in each condition is depicted through whiskers. The findings illustrate that the synchronous integration of motion cues with visual cues reduces the severity of motion sickness.

When comparing motion sickness scores while simulating only visual cues C1(No Motion) to visual–vestibular cues (C2–C6), the severity of motion sickness alleviates by 31% in the case of the roll mission profile. Similarly, the severity of motion sickness reduces by

21%, in the pitch mission profile when only visual cues are replaced with visual–vestibular cues. For each pairwise comparison in the Tukey post hoc analysis, the confidence interval does not encompass the zero value, revealing that each condition significantly affects motion sickness.

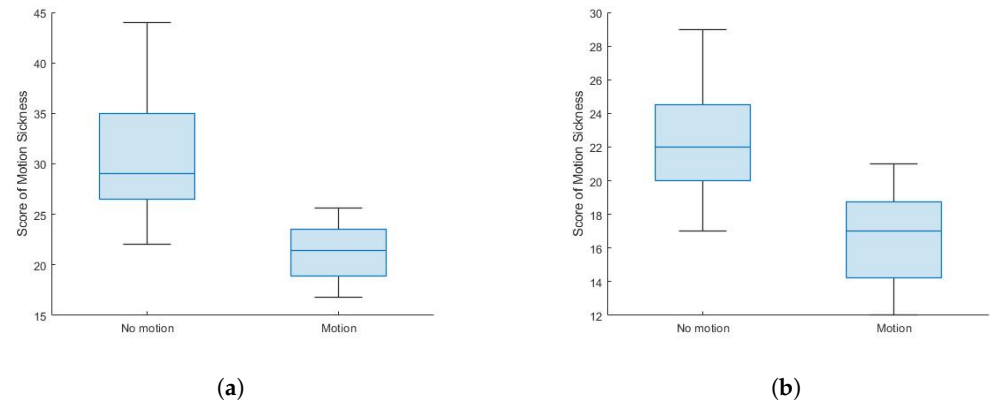


Figure 9. (a) Comparison of the score of motion sickness experienced with and without motion cues across the roll mission profile. (b) Comparison of the score of motion sickness experienced with and without motion cues across the pitch mission profile.

4.2. Effect on Motion Sickness across Different Ratios of Visual–Vestibular Conditions

Using the results generated from simulating all six conditions (C1, C2, C3, C4, C5, C6) across two mission profiles, i.e., roll and pitch, a one-way ANOVA analysis was performed to analyze whether there is a significant effect on the score of motion sickness across all six conditions. The results revealed significant effects for both the roll mission profile, $F(5, 24) = 2.62$ with effect size = 0.508, and the pitch mission profile, $F(5, 24) = 2.62$ with effect size = 0.315.

A one-Way ANOVA = was performed for one-to-one comparison of the no-motion condition (C1) to five other conditions (C2–C6) across the roll mission profile. Similarly, the test was repeated to determine significant differences across the two conditions (C1/C2–C6) in the pitch mission profile. The statistical analysis for the roll and pitch mission profiles is shown in Table 5.

Table 5. Statistical analysis of models generated by comparison of C1 with (C2–C6) for roll and pitch mission profiles.

Comparison Models of No Motion Condition (C1) with	Effect Size	F-Value	p-Value
Roll Mission Profile			
C2 (Log)	0.037	0.640	0.446
C3 (Expo)	0.481	10.269	0.012
C4 (Gain $\times 0.5$)	0.361	6.664	0.032
C5 (Gain $\times 2$)	0.135	2.568	0.147
C6 (Synchronous)	0.616	17.065	0.003
Pitch Mission Profile			
C2 (Log)	0.108	0.020	0.890
C3 (Expo)	0.337	6.101	0.038
C4 (Gain $\times 0.5$)	0.179	3.181	0.112
C5 (Gain $\times 2$)	0.109	2.234	0.173
C6 (Synchronous)	0.508	14.835	0.004

An illustrative representation of the one-way analysis of variance (ANOVA) for roll and pitch mission profiles was captured through box plots. A statistical summary of potential outliers with the interquartile range is presented in Figure 10. Distinctive differences in means of motion sickness across various ratios of visual–vestibular cues are evident, invalidating the null hypothesis. As shown in Figure 10, in both the roll and pitch profiles, the synchronized conditions always resulted in lower reports of simulator sickness compared to any of the other conditions. Similarly, the no-motion conditions were always associated with worse simulator sickness when compared to any of the other motion conditions. The ranking of motion sickness severity across diverse ratios of visual–vestibular conditions for the roll and pitch mission profiles can also be represented based on the sum of individual user feedbacks across six visual–vestibular conditions, visually displayed in Figure 11.

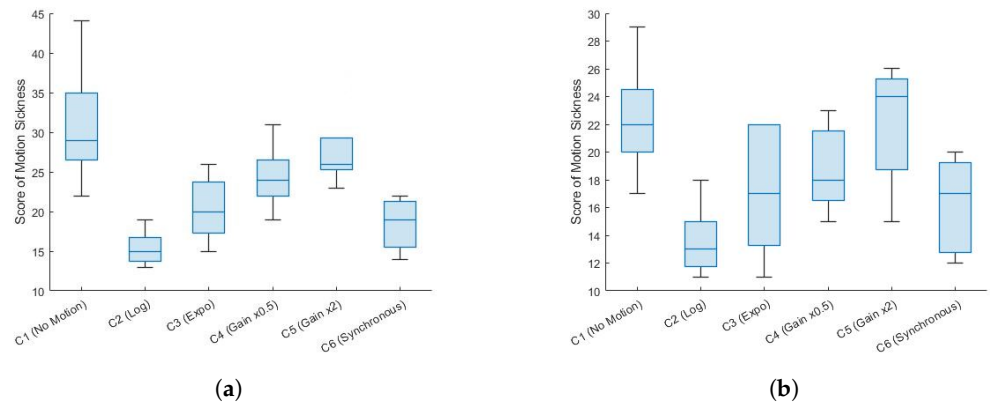


Figure 10. (a) Box plot representation of score of motion sickness across all six visual–vestibular conditions for roll mission profile. (b) Box plot representation of score of motion sickness across all six visual–vestibular conditions for pitch mission profile.

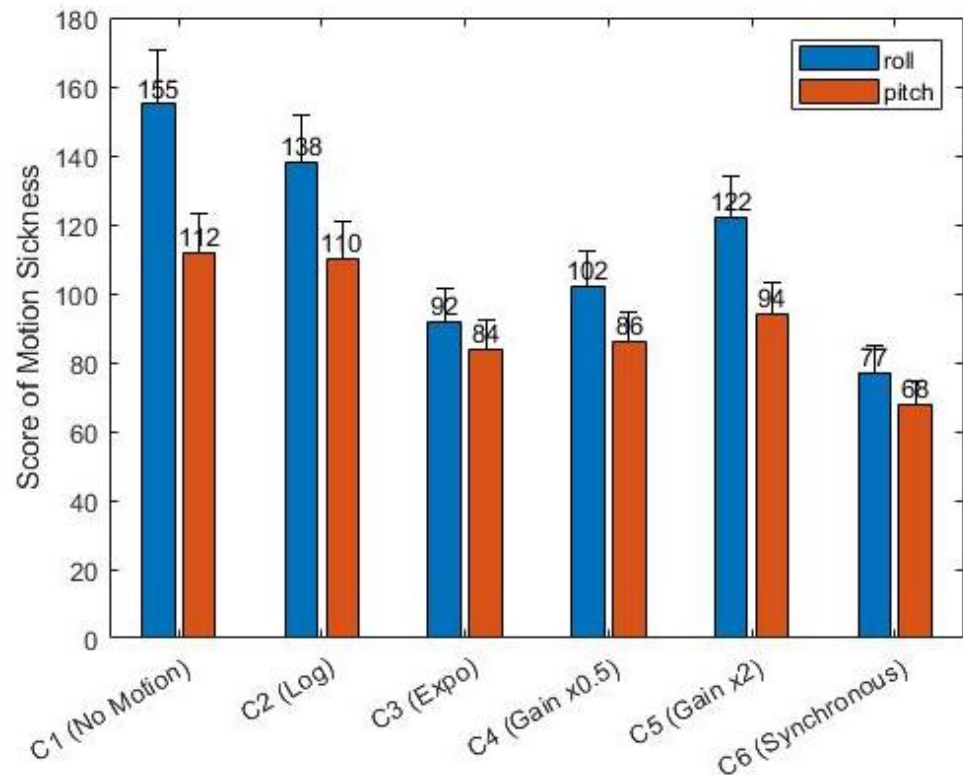


Figure 11. Comparison of score of motion sickness across all six ratios of visual–vestibular conditions in roll and pitch mission profile.

4.3. Impact on SSQ Sub-Scores under Different Ratios of Visual–Vestibular Cues

The total motion sickness score was categorized into sub-scores of nausea (N), disorientation (D), and oculomotor (O). Independent models were generated to analyze the SSQ sub-score categories across six different visual and vestibular condition ratios. Each model is confined to a particular SSQ sub-score category generated against each visual–vestibular condition when simulated with roll or pitch mission profiles. For example, Model M1 is the score of nausea experienced by users across all six ratios of visual–vestibular cues during the virtual simulation of a pitch mission profile. Similarly, the six models generated to analyze SSQ sub-score categories across roll and pitch mission profiles were:

- M1: Score of nausea during pitch mission profile for all six ratios of visual–vestibular cues.
- M2: Score of oculomotor during pitch mission profile for all six ratios of visual–vestibular cues.
- M3: Score of disorientation during pitch mission profile for all six ratios of visual–vestibular cues.
- M4: Score of nausea during roll mission profile for all six ratios of visual–vestibular cues.
- M5: Score of oculomotor during roll mission profile for all six ratios of visual–vestibular cues.
- M6: Score of disorientation during roll mission profile for all six ratios of visual–vestibular cues.

The results found that condition M1 ($F = 5.35, p = 0.02 < \alpha$), condition M2 ($F = 3.30, p = 0.021 < \alpha$), condition M3 ($F = 2.26, p = 0.041 < \alpha$), condition M4 ($F = 2.7, p = 0.042 < \alpha$), condition M5 ($F = 5.35, p = 0.002 < \alpha$), and condition M6 ($F = 8.32, p = 0.0006 < \alpha$) have a significant effect on motion sickness. The p -values lie within the 95% confidence interval.

The subjective motion sickness severity was assessed through non-mutually exclusive categories, representing nausea (N), oculomotor disturbance (O), and disorientation (D). Each symptom in the SSQ was weighted by its loading factor [42], and category scores were determined by summing the weighted symptom scores multiplied by a constant scaling factor. The overall motion sickness score was calculated as the sum of scores from each category, each multiplied by a constant factor [43].

The findings underscore a notable discrepancy in the severity of motion sickness between the roll and pitch mission profiles, with the roll mission profile exhibiting a higher severity level. The comprehensive cybersickness profile across sub-categories can be hierarchically arranged: disorientation > oculomotor > nausea. This profiling reflects the severity and frequency of these distinct syndromes within the context of motion sickness.

Each SSQ sub-category score was measured across multiple ranges of visual–vestibular conditions. The results show that the severity of nausea, oculomotor, and disorientation across different ratios of visual–vestibular information follows the same order as that of the total motion sickness score across all six ratios of the visual–vestibular sensory interface, as shown in Figures 12–15.

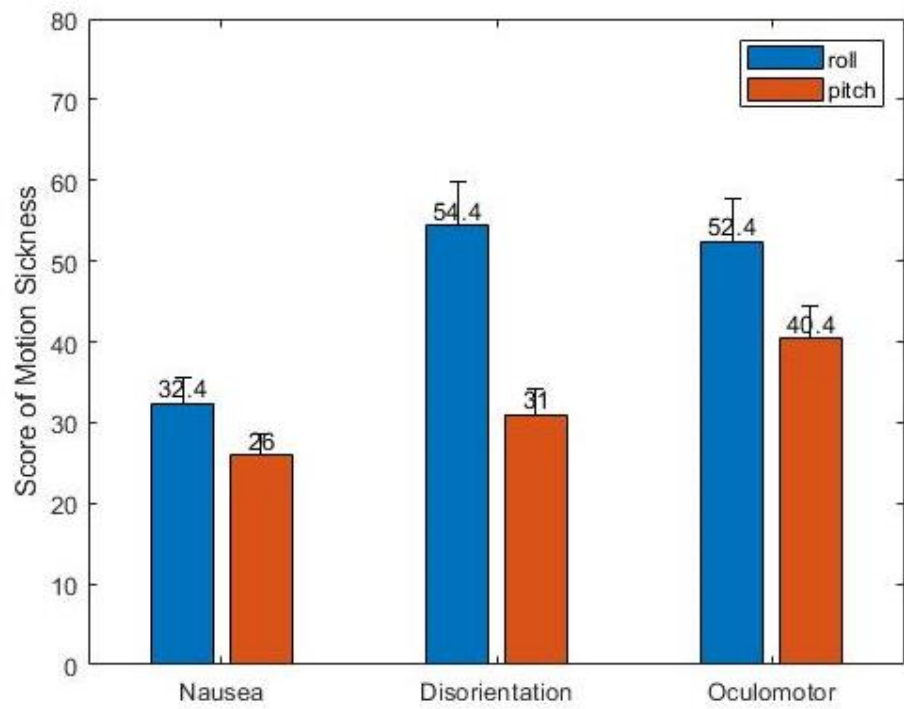


Figure 12. Overall score of SSQ sub-categories.

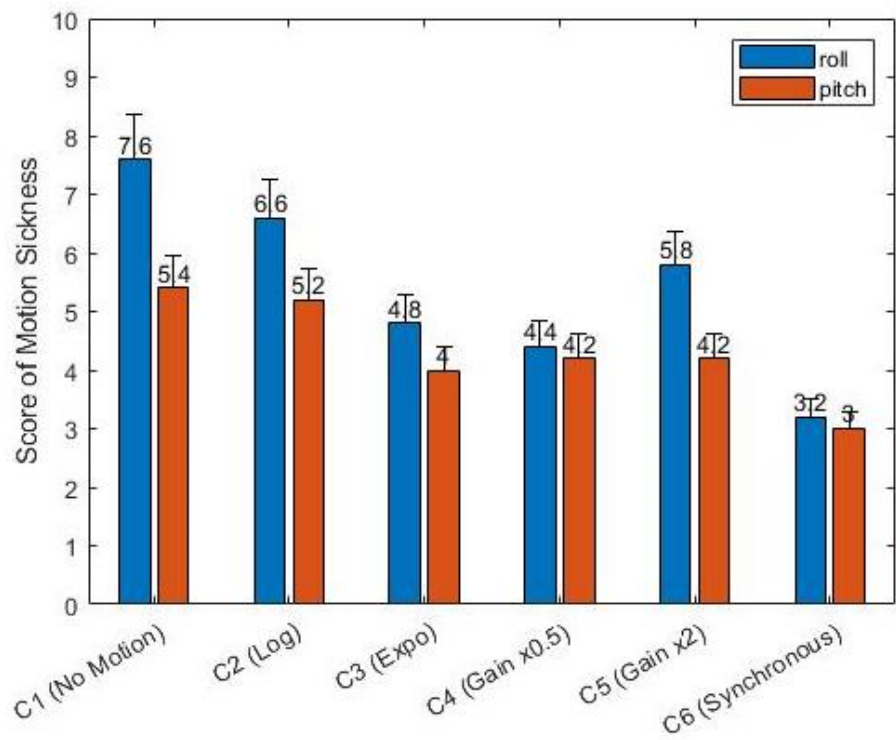


Figure 13. Score of nausea across multiple ratios of visual-vestibular cues.

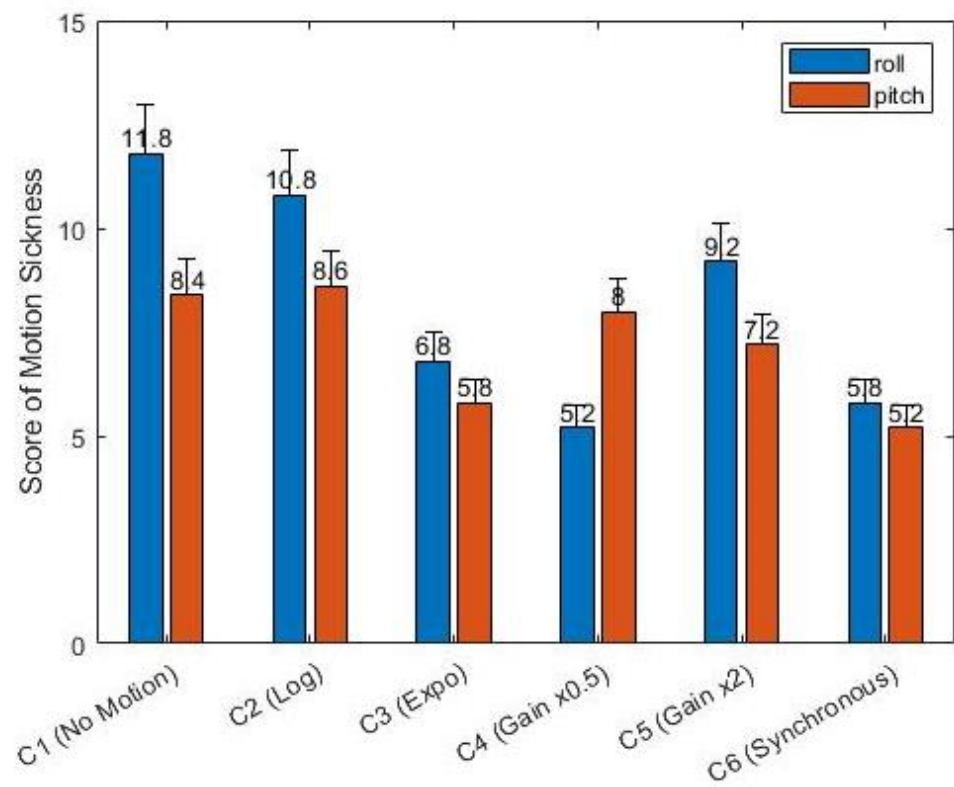


Figure 14. Score of oculomotor across multiple ratios of visual–vestibular cues.

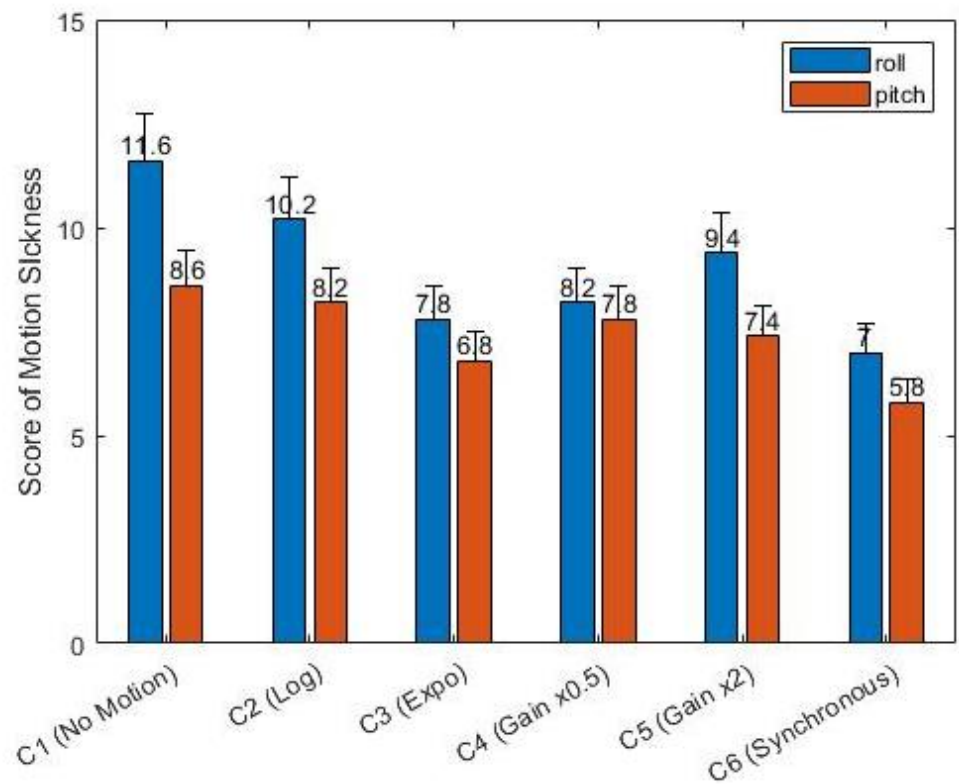


Figure 15. Score of disorientation across multiple ratios of visual–vestibular cues.

4.4. Incidental Findings

This study aimed to analyze motion sickness under multiple ratios of visual–vestibular stimuli using a 2-degree-of-freedom virtual reality (VR) motion simulator. Participants who skipped breakfast showed a motion sickness score variation of 2% and 3% in the pitch and roll mission profiles, respectively, compared to the average score of motion sickness in other participants. This indicates that skipping breakfast does not affect motion sickness if an ample number of calories were consumed during the last meal. Motion sickness was more pronounced during the roll mission profile than during the pitch mission profile. It was observed that adding vestibular stimuli to the stereoscopic visual cues reduces the amount of motion sickness by 31% and 21% during roll and pitch mission profiles, respectively. The synchronous visual–vestibular cues exhibited the most minor severity of motion sickness. The identified hierarchy of motion sickness severity across conditions [C1 (No Motion) > C2 (Log) > C5 (Gain \times 2) > C4 (Gain \times 0.5) > C3 (Expo) > C6 (Synchronous)] offers valuable insights for optimizing VR-based flight-simulation setups. This reflects that motion sickness increases with an increasing disparity in the inputs of visual and vestibular cues. This experiment reaffirms the existing research by establishing that disorientation holds greater significance than oculomotor discomfort and nausea in contributing to motion sickness. The consistent cybersickness profile—disorientation > oculomotor > nausea—shown in Figure 12, in both roll and pitch mission profiles, also supports the literature [17]. This study sheds light on the nuanced dynamics of visual–vestibular interactions in mitigating motion sickness within a VR flight-simulation context, providing a foundation for further research and optimizing VR-based training setups for pilots and UAV operators.

5. Conclusions

In this study, we developed a 2-degree-of-freedom (2DoF) virtual reality (VR) motion simulator to evaluate the intricate interplay between in-phase and out-of-phase visual–vestibular sensory interactions. The findings reveal that inertial cues are pivotal in mitigating motion sickness, resulting in 21% and 31% reductions in the pitch and roll mission profiles, respectively. Notably, the attenuation of motion sickness in the pitch mission profile was ineffective compared to the roll mission profile. The positive correlation observed between motion sickness and motion cues shows that visual–vestibular cues are two facets of the virtual experience that enhance the overall virtual experience when synchronized.

The subjective assessment of motion sickness scores in six varied visual–vestibular conditions indicated that the condition characterized by harmoniously synchronized visual–vestibular sensory stimuli denoted as C6 (Synchronous) recorded the least motion sickness score. Conversely, when there was no motion stimulus and only visual cues were simulated, represented by condition C1 (No Motion), the maximum score of motion sickness experienced was recorded. Condition C2 (Log), characterized by combining motion cues with visual inputs but within a limited range, resulting in a pronounced ratio difference, recorded a significantly lower motion sickness severity than condition C1 (No Motion). This underscores synchronized and congruent sensory cues' pivotal role in effective motion sickness alleviation.

Furthermore, when a substantial phase discrepancy exists between the visual viewport rotation and physical rotation, such as observed in condition C4 (Gain \times 0.5), the motion sickness severity escalates—albeit to a lesser extent than the absence of motion stimuli. The overarching hierarchy of motion sickness for both roll and pitch mission profiles is C1 (No Motion) > C2 (Log) > C5 (Gain \times 2) > C4 (Gain \times 0.5) > C3 (Expo) > C6 (Synchronous).

This comprehensive analysis extends to a comparative examination of sub-category scores within the Simulator Sickness Questionnaire (SSQ), encompassing nausea, oculomotor, and disorientation. The findings reaffirm prior studies, where motion sickness induced by nausea was of a lesser magnitude than the effects of oculomotor and disorientation. Our study's cybersickness profile follows the order disorientation > oculomotor > nausea. This hierarchical order is maintained even within the context of differing motion sickness severity scores between the roll and pitch mission profiles.

Author Contributions: Conceptualization, S.R. and A.M.; Formal analysis, A.J. and S.R.; Investigation, A.J., S.R. and A.M.; Resources, A.M.; Writing—original draft, A.J.; Writing—review & editing, A.J., S.R. and A.M.; Supervision, S.R. and A.M.; Project administration, A.M.; Funding acquisition, A.M. All authors have read and agreed to the published version of the manuscript.

Funding: This research received no external funding.

Informed Consent Statement: Informed Consent was obtained from all subjects involved in this study.

Data Availability Statement: The data presented in this study are available on request from the corresponding author.

Acknowledgments: The authors want to acknowledge the Computational Aeronautics Lab (CAL) and the Hub of Immersive Virtual Environments (HIVE) at NUST, Pakistan, for providing research facilities.

Conflicts of Interest: The authors declare no conflict of interest. There was no external received in this research.

Nomenclature

Latin Symbols

E_a	Back EMF induced in the Motor (V)
R_a	Armature Resistance of the Motor (ω)
L_a	Armature Inductance of the Motor (H)
K_b	Back EMF Constant of the Motor (V)
T_L	Torque Load of the Motor (τ)
K_g	Internal Gear Reduction Constant
K_p	Proportionality Constant
K_i	Integration Constant
K_d	Differential Constant

Greek Symbols

τ_{pitch}	Equivalent Pitch Torque (τ)
τ_{roll}	Equivalent Roll Torque (τ)
ω_m	Angular velocity of the Motor (rev/min)
α	Significance Level

Subscripts

$\rightarrow F_{pitch}$	Equivalent Pitch Force Required (N)
$\rightarrow F_{roll}$	Equivalent Roll Force Required (N)
J	Inertia of the Motor ($\text{kg}\cdot\text{m}^2$)
J_{eq}	Equivalent Inertia of the Motion Platform ($\text{kg}\cdot\text{m}^2$)

Abbreviations

DoF	Degree of Freedom
VR	Virtual Reality
SSQ	Simulator Sickness Questionnaire
GPU	Graphics Processing Unit
HMD	Head-Mounted Display
UDP	User Datagram Protocol
CNS	Central Nervous System
ANOVA	Analysis of Variance

References

1. Sherman, B.; Durlach, N.I.; Mavor, A.S. (Eds.) *Virtual Reality: Scientific and Technological Challenges*; National Academy Press: Washington, DC, USA, 1995; 542p, ISBN 0 309 05135 5 (hbk). [[CrossRef](#)]
2. Keshavarz, B.; Hecht, H.; Zschuschke, L. Intra-visual conflict in visually induced motion sickness. *Displays* **2011**, *32*, 181–188. [[CrossRef](#)]
3. Kennedy, R.; Berbaum, K.; Lilienthal, M.; Dunlap, W.; Mulligan, B. *Guidelines for Alleviation of Simulator Sickness Symptomatology*; Technical Report; Naval Training Systems Center: Orlando, FL, USA, 1987.
4. Bos, J.E.; Bles, W.; Groen, E.L. A theory on visually induced motion sickness. *Displays* **2008**, *29*, 47–57. [[CrossRef](#)]
5. Burdea, G.C.; Coiffet, P. *Virtual Reality Technology*; John Wiley & Sons: Hoboken, NJ, USA, 2003.

6. Hill, K.J.; Howarth, P.A. Habituation to the side effects of immersion in a virtual environment. *Displays* **2000**, *21*, 25–30. [[CrossRef](#)]
7. Keshavarz, B.; Riecke, B.E.; Hettlinger, L.J.; Campos, J.L. Vection and visually induced motion sickness: How are they related? *Front. Psychol.* **2015**, *6*, 472. [[CrossRef](#)]
8. Rebenitsch, L.; Owen, C. Review on cybersickness in applications and visual displays. *Virtual Real.* **2016**, *20*, 101–125. [[CrossRef](#)]
9. Kurniawan, C.; Rosmansyah, Y.; Dabarsyah, B. A systematic literature review on virtual reality for learning. In Proceedings of the 2019 IEEE 5th International Conference on Wireless and Telematics (ICWT), Yogyakarta, Indonesia, 25–26 July 2019; pp. 1–4.
10. Zaghloul, H. An Exploratory Study on The Use of 3d Hologram Visualization in Egypt’s Educational Theater. *Educ. Inf. Technol.* **2020**, *14*, 32–44. [[CrossRef](#)]
11. Golding, J.F. Motion sickness. *Handb. Clin. Neurol.* **2016**, *137*, 371–390.
12. Aykent, B.; Merienne, F.; Guillet, C.; Paillot, D.; Kemeny, A. Motion sickness evaluation and comparison for a static driving simulator and a dynamic driving simulator. *Proc. Inst. Mech. Eng. Part J. Automob. Eng.* **2014**, *228*, 818–829. [[CrossRef](#)]
13. Keshavarz, B.; Ramkhalawansingh, R.; Haycock, B.; Shahab, S.; Campos, J. Comparing simulator sickness in younger and older adults during simulated driving under different multisensory conditions. *Transp. Res. Part Traffic Psychol. Behav.* **2018**, *54*, 47–62. [[CrossRef](#)]
14. Casas, S.; Portalés, C.; Fernández, M. To move or not to move?: The challenge of including believable self-motion cues in virtual reality applications—understanding motion cueing generation in virtual reality. In *Cases on Immersive Virtual Reality Techniques*; IGI Global: Hershey, PA, USA, 2019; pp. 124–144.
15. Dziuda, L.; Biernacki, M.; Baran, P.; Truszczyński, O. The effects of simulated fog and motion on simulator sickness in a driving simulator and the duration of after-effects. *Appl. Ergon.* **2014**, *45*, 406–412. [[CrossRef](#)]
16. Dongsu, W.; Hongbin, G. Adaptive sliding control of six-DOF flight simulator motion platform. *Chin. J. Aeronaut.* **2007**, *20*, 425–433. [[CrossRef](#)]
17. Ng, A.K.; Chan, L.K.; Lau, H.Y. A study of cybersickness and sensory conflict theory using a motion-coupled virtual reality system. *Displays* **2020**, *61*, 101922. [[CrossRef](#)]
18. Herpers, R.; Heiden, W.; Kutz, M.; Scherfgen, D.; Hartmann, U.; Bongartz, J.; Schulzyk, O. FIVIS bicycle simulator: An immersive game platform for physical activities. In Proceedings of the 2008 Conference on Future Play: Research, Play, Share, Toronto, ON, Canada, 3–5 November 2008; pp. 244–247.
19. Teasdale, N.; Lavallièrre, M.; Tremblay, M.; Laurendeau, D.; Simoneau, M. Multiple exposition to a driving simulator reduces simulator symptoms for elderly drivers. In *Driving Assessment Conference*; University of Iowa: Iowa City, IA, USA, 2009; Volume 5.
20. Howarth, P.A.; Hodder, S.G. Characteristics of habituation to motion in a virtual environment. *Displays* **2008**, *29*, 117–123. [[CrossRef](#)]
21. DiZio, P.; Lackner, J.R. Circumventing side effects of immersive virtual environments. *Adv. Hum. Factors/Ergon.* **1997**, *21*, 893–896.
22. Kolasinski, E.M. *Simulator Sickness in Virtual Environments*; US Army Research Institute for the Behavioral and Social Sciences: Alexandria, VA, USA, 1995; Volume 1027.
23. Pausch, R.; Crea, T.; Conway, M. A literature survey for virtual environments: Military flight simulator visual systems and simulator sickness. *Presence Teleoperators Virtual Environ.* **1992**, *1*, 344–363. [[CrossRef](#)]
24. Yao, R.; Heath, T.; Davies, A.; Forsyth, T.; Mitchell, N.; Hoberman, P. Oculus vr best practices guide. *Oculus VR* **2014**, *4*, 27–35.
25. Tal, D.; Gonen, A.; Wiener, G.; Bar, R.; Gil, A.; Nachum, Z.; Shupak, A. Artificial horizon effects on motion sickness and performance. *Otol. Neurotol.* **2012**, *33*, 878–885. [[CrossRef](#)]
26. Bos, J.E.; MacKinnon, S.N.; Patterson, A. Motion sickness symptoms in a ship motion simulator: Effects of inside, outside, and no view. *Aviat. Space Environ. Med.* **2005**, *76*, 1111–1118.
27. Feenstra, P.; Bos, J.E.; van Gent, R.N. A visual display enhancing comfort by counteracting airsickness. *Displays* **2011**, *32*, 194–200. [[CrossRef](#)]
28. Cao, Z.; Jerald, J.; Kopper, R. Visually-induced motion sickness reduction via static and dynamic rest frames. In Proceedings of the 2018 IEEE Conference on Virtual Reality and 3D User Interfaces (VR), Tuebingen/Reutlingen, Germany, 18–22 March 2018; pp. 105–112.
29. Fernandes, A.S.; Feiner, S.K. Combating VR sickness through subtle dynamic field-of-view modification. In Proceedings of the 2016 IEEE Symposium on 3D User Interfaces (3DUI), Greenville, SC, USA, 19–20 March 2016; pp. 201–210.
30. Nguyen-Vo, T.; Riecke, B.E.; Stuerzlinger, W. Simulated reference frame: A cost-effective solution to improve spatial orientation in vr. In Proceedings of the 2018 IEEE Conference on Virtual Reality and 3D User Interfaces (VR), Tuebingen/Reutlingen, Germany, 18–20 March 2018; pp. 415–422.
31. Whittinghill, D.M.; Ziegler, B.; Case, T.; Moore, B. Nasum virtualis: A simple technique for reducing simulator sickness. In Proceedings of the Games Developers Conference (GDC), San Francisco, CA, USA, 2–6 March 2015; Volume 74.
32. Oman, C.M. A heuristic mathematical model for the dynamics of sensory conflict and motion sickness. *Acta Oto-Laryngol.* **1982**, *94*, 4–44. [[CrossRef](#)]
33. Lin, C.T.; Chuang, S.W.; Chen, Y.C.; Ko, L.W.; Liang, S.F.; Jung, T.P. EEG effects of motion sickness induced in a dynamic virtual reality environment. In Proceedings of the 2007 29th Annual International Conference of the IEEE Engineering in Medicine and Biology Society, Lyon, France, 22–26 August 2007; pp. 3872–3875.

34. Llorach, G.; Evans, A.; Blat, J. Simulator sickness and presence using HMDs: Comparing use of a game controller and a position estimation system. In Proceedings of the 20th ACM Symposium on Virtual Reality Software and Technology, Edinburgh, UK, 11–13 November 2014; pp. 137–140.
35. Ash, A.; Palmisano, S.; Kim, J. Vection in depth during consistent and inconsistent multisensory stimulation. *Perception* **2011**, *40*, 155–174. [[CrossRef](#)]
36. Peck, T.C.; Fuchs, H.; Whitton, M.C. An evaluation of navigational ability comparing redirected free exploration with distractors to walking-in-place and joystick locomotion interfaces. In Proceedings of the 2011 IEEE Virtual Reality Conference, Singapore, 19–23 March 2011; pp. 55–62.
37. Banton, T.; Stefanucci, J.; Durgin, F.; Fass, A.; Proffitt, D. The Perception of Walking Speed in a Virtual Environment. *Presence* **2005**, *14*, 394–406. [[CrossRef](#)]
38. Schroeder, J.A. *Helicopter Flight Simulation Motion Platform Requirements*; Technical Report; NASA: Washington, DC, USA, 1999.
39. Grant, P.R.; Yam, B.; Hosman, R.; Schroeder, J.A. Effect of simulator motion on pilot behavior and perception. *J. Aircr.* **2006**, *43*, 1914–1924. [[CrossRef](#)]
40. Stanney, K.M.; Hale, K.S.; Nahmens, I.; Kennedy, R.S. What to expect from immersive virtual environment exposure: Influences of gender, body mass index, and past experience. *Hum. Factors* **2003**, *45*, 504–520. [[CrossRef](#)] [[PubMed](#)]
41. Mazloumi Gavvani, A.; Walker, F.R.; Hodgson, D.M.; Nalivaiko, E. A comparative study of cybersickness during exposure to virtual reality and “classic” motion sickness: Are they different? *J. Appl. Physiol.* **2018**, *125*, 1670–1680. [[CrossRef](#)]
42. Balk, S.A.; Bertola, D.B.; Inman, V.W. Simulator sickness questionnaire: Twenty years later. In *Driving Assessment Conference*; University of Iowa: Iowa City, IA, USA, 2013; Volume 7.
43. Bimberg, P.; Weissker, T.; Kulik, A. On the usage of the simulator sickness questionnaire for virtual reality research. In Proceedings of the 2020 IEEE Conference on Virtual Reality and 3D User Interfaces Abstracts and Workshops (VRW), Atlanta, GA, USA, 22–26 March 2020; pp. 464–467.

Disclaimer/Publisher’s Note: The statements, opinions and data contained in all publications are solely those of the individual author(s) and contributor(s) and not of MDPI and/or the editor(s). MDPI and/or the editor(s) disclaim responsibility for any injury to people or property resulting from any ideas, methods, instructions or products referred to in the content.